Fabrication and structural performance of periodic cellular metal sandwich structures

Haydn N.G. Wadley[a],*, Norman A. Fleck[b], Anthony G. Evans[c]

[a]Department of Materials Science and Engineering, University of Virginia, Charlottesville, Virginia, 22903, USA
[b]Engineering Department, University of Cambridge, UK
[c]Department of Materials Science and Engineering, University of California at Santa Barbara, Santa Barbara, California, USA

Abstract

Metallic sandwich panels with periodic, open-cell cores are important new structures, enabled by novel fabrication and topology design tools. Fabrication protocols based on the sheet forming of trusses and shell elements (egg-boxes) as well as textile assembly have allowed the manufacture of robust structures by inexpensive routes. Topology optimization enables control of failure mechanisms at the truss length scale, leading to superior structural performance. Analysis, testing and optimization have demonstrated that sandwich panels constructed with these cores sustain loads at much lower relative densities than stochastic foams. Moreover, the peak strengths of truss and textile cores are superior to honeycombs at low relative densities, because of their superior buckling resistance. Additional benefits of the truss/textile cores over honeycombs reside in their potentially lower manufacturing cost as well as in their multifunctionality.
© 2003 Elsevier Ltd. All rights reserved.

1. Introduction

Numerous techniques have been developed for synthesizing inexpensive metal foams with stochastic, closed cells [1,2]. Other processes have been devised for manufacturing open cell, stochastic structures [3–10]. Some utilize open cell polymer templates for investment casting [4,5], chemical vapor deposition [6] or slurry coating [7]. Others utilize hollow spheres [8–10] or aggregates of soluble particles into which metals can be injected and solidified [11]. A leaching process removes the template leaving behind a cellular solid. While potentially less expensive to fabricate than benchmark honeycomb systems, their mechanical performance is greatly inferior, because the metal ligaments experience bending when loaded [12]. Moreover, most have an as-cast ligament microstructure that contributes to low ductility [13].

Besides their load bearing function,most cellular metals have multifunctional potential. (i) They can be good energy absorbers during impact loading [1]. (ii) Some closed cell systems afford thermal isolation opportunities [1] and others can be good sound dampers [14]. (iii) Open cell materials have been used as cross flow heat exchangers [15], as current collectors for nickel metal hydride batteries [6] and as catalyst supports [16].

The inferior structural performance of stochastic systems has spurred interest in periodic cellular metals (PCMs) that not only compete with honeycombs (Fig. 1),
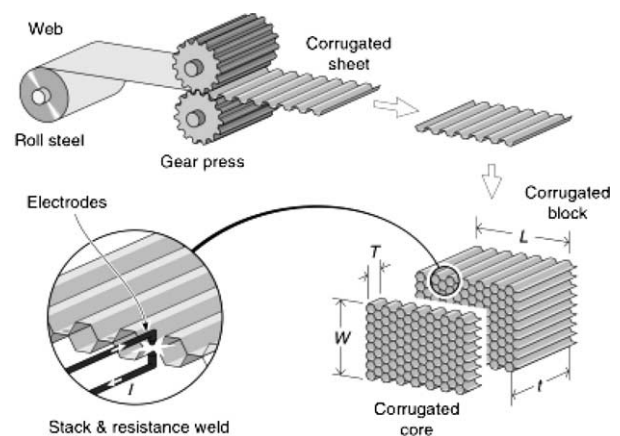

Fig. 1. Low relative density metallic honeycomb cores for sandwich panels can be made by a sheet crimping process.The stacked sheets can be bonded by resistance welding (shown) or with an adhesive.The cores can be cut and adhesively bonded to face sheets to create sandwich panels.

* Corresponding author. Tel.: +1-804-982-5670; fax: +1-804-824-2032.
  E-mail address: haydn@virginia.edu (H.N.G. Wadley).

but also offer multifunctionality [17]. The benefits arise when PCMs are configured as cores within sandwich structures that experience either bending or compression [18,19]. The cores of interest can comprise either prismatic elements (honeycomb, textile and corrugations) or an assembly of struts (tetrahedral, pyramidal, Kagome) or shell elements (egg-box). The truss and textile topologies (Fig. 2) can have either solid or hollow ligaments. This review emphasizes the preferred fabrication methods and the conceptual basis for topology selection, as well as the attributes of the best load supporting structures.

2. Manufacturing methods

The emergence of periodic cellular core panel structures has been paced by the development of a variety of casting, forming and textile techniques that enable topology control [20]. Each approach has strengths and limitations for fabricating the topologies shown in Fig. 2.

2.1. Investment casting

Truss core patterns with attached face sheets can be made from a volatile wax or polymer (eg polyurethane) by injection molding [21] or rapid prototyping methods [22].This pattern, together with a system of gating and risers, is coated with a ceramic casting slurry and dried. The wax or polymer is removed by melting or vaporization and the empty mold filled with liquid metal. Lattice block [23], and more recently pyramidal, tetrahedral [22] and 3D Kagome [18] core structures have each been made in this manner (Fig. 3). The approach allows the fabrication of complex, non-planar shapes. Moreover, with the advent of rapid prototyping,

casting pattern manufacture can be automated. However, structures with near-optimal, low-relative-density cores are difficult to fabricate because of the tortuous metal paths and the resulting susceptibility to casting defects. The need to infiltrate the tortuous structure also limits the process to alloys having high fluidity. Aluminum/silicon [21], copper/beryllium [18] and IN 718 superalloy [24] have been used to date. The aluminum/silicon alloys suffer from low ductility, which impairs structural robustness.

2.2. Deformation forming

Egg-box topologies of low relative density can be fabricated from high formability alloys by a simple press forming operation.In plan view, the tetrahedral truss core has a hexagonal pattern with alternate nodes displaced above or below the plane. A single layer truss core can therefore be made by perforating a sheet to create a pattern and then bending at the nodes (Fig. 4) [25]. A pyramidal core can be made by starting with
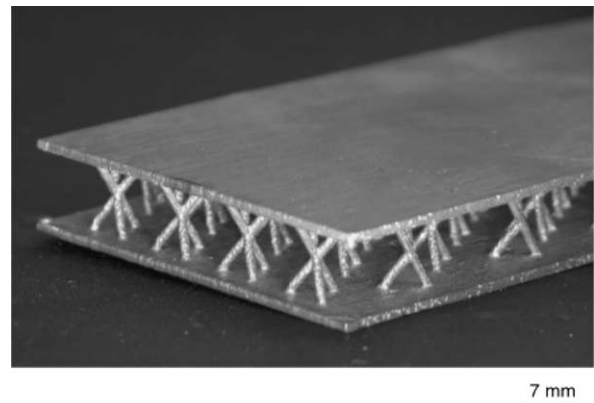

7 mm

Fig. 3. An example of an investment cast 3D Kagome sandwich panel.The alloy was Cu-1.8%Be and the core relative density was 2%.
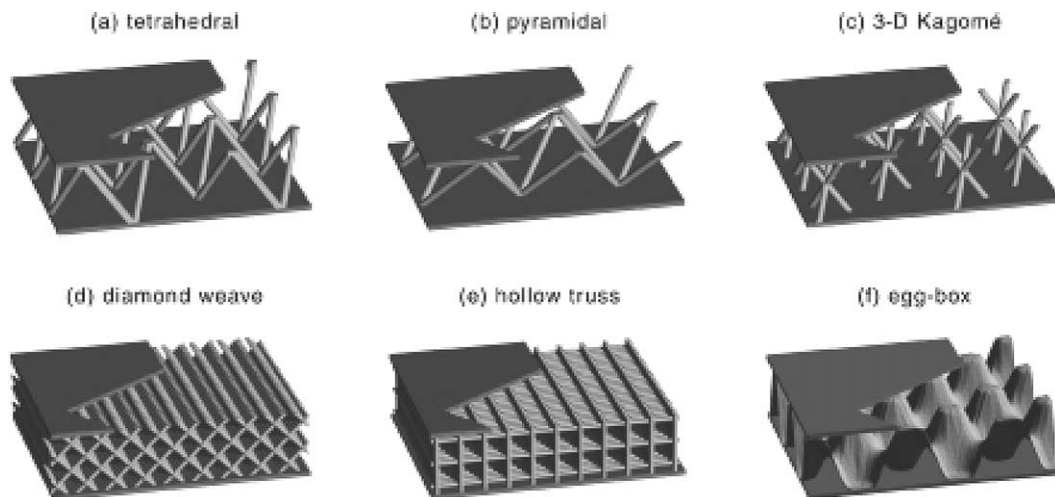

Fig. 2. Examples of sandwich panels with periodic cellular metal cores. The different topologies can be optimized for specific loads by identifying the topology dependent failure modes and manipulating the geometry to suppress the performance-limiting mechanisms.

a diamond perforation. These truss layers can be used as basic units to create a variety of materials and structures.

1. Stacked node-to-node and bonded to create a lattice block of cellular material.
2. Interleaved with perforated or solid sheets.
3. Used as cores of sandwich panels with either solid faces or faces having triangular or hexagonal cut-outs (Fig. 5).

Many bonding processes are available to fabricate these structures with robust nodes. For some materials, resistance welding can be used. For titanium alloys diffusion bonding has been successful. Brazing methods can be used for aluminum alloys. For many stainless steels, superalloys and copper alloys a transient liquid phase (TLP) process can be used [2].

Transient liquid phase bonding involves coating (by dipping or spraying) the materials to be bonded with an alloy dispersed in a binder/adhesive. Many such materials have been developed. For example, the Ni/25Cr/10P alloy is applicable to stainless steels. After application of the bonding agent, the system is heated to a moderate temperature to remove the binder. It is then heated to the melting temperature of the transient liquid phase. Capillary forces draw much of the fluid to the nodes. Interdiffusion with the host metal changes the liquid composition over time and raises its solidus temperature, enabling it to solidify. The resulting nodes have strength and ductility comparable to the parent material. An example of a tetrahedral truss core sandwich panel made by this route is shown in Fig. 6 (upper) [25]. In this example, the core relative density is 1.8%. The lower micrograph shows a higher magnification view of a node. This approach creates a structure comprising an annealed, wrought alloy that exhibits
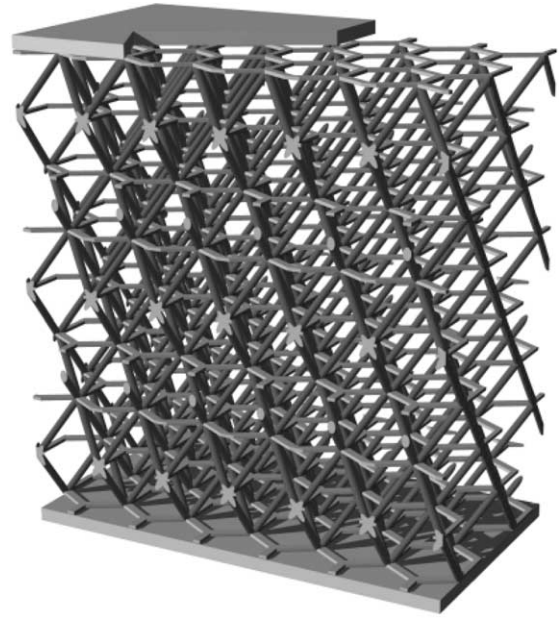

Fig. 5. An example of a periodic cellular lattice. In this case layers of a tetrahedral structure are stacked node to node with an interleaved planar hexagonal perforated layer. Many other topologies can be made by similar construction. Cell sizes of a millimeter to several centimeters can be made by deformation forming and subsequent assembly.
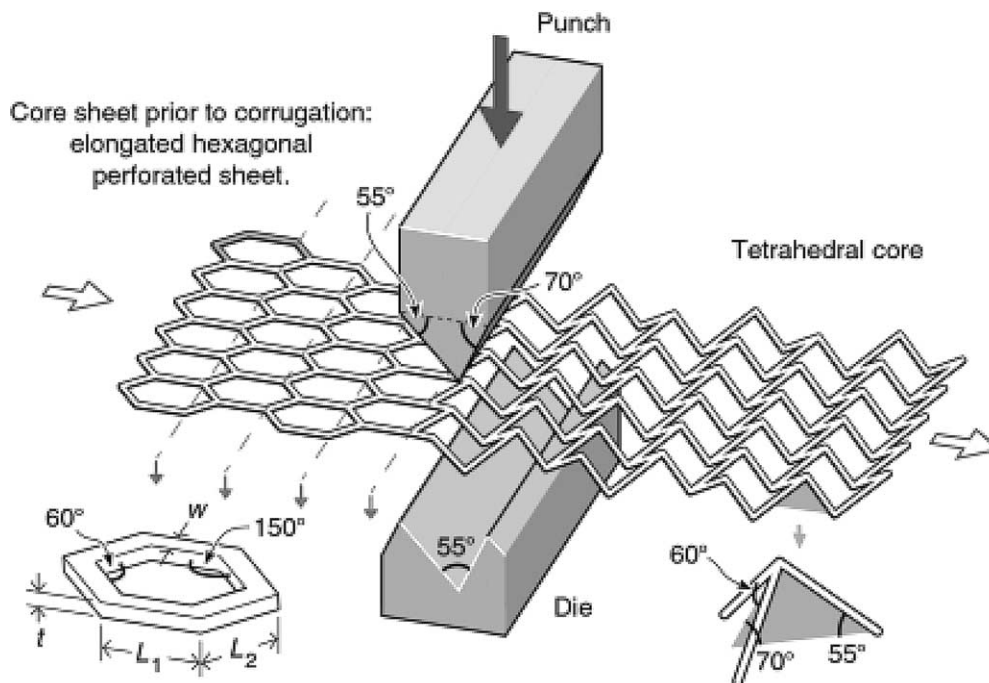

Fig. 4. A tetrahedral truss core can be made by bending the nodes of a stretched hexagonal perforated metal sheet. The case shown corresponds to the octet truss topology with a truss angle of 55°.

much greater ductility than their investment cast counterparts.

The constructed metal lattice approach has the limitation that sheet perforation results in the inefficient use of material. Other approaches have therefore been explored. They are based upon the use of metal wires and tubes, described next.

2.3. Metal wire approaches

2.3.1. Textiles

Metal textile technology is well developed and a mature technology base exists. Weaving, braiding and sewing provide simple, inexpensive methods for controlling positions. The approaches are applicable to any alloy that can be drawn into wire. Tubes are more difficult to weave because of their high bending resistance and propensity to asymmetric buckling when plastically bent. Plain weave 0/90 fabrics are the simplest to envision. The included angle is readily modified after weaving by shearing the fabric. A wide range of the cell width/fiber diameter ratio is accessible. The upper limit is established by fabric stability. That is, small diameter wires with large cell diameter remain elastic during weaving such that the associated forces disrupt the spacing during handling. Precrimping the wire before weaving or spot welding some nodes after fabric manufacture can solve this problem.
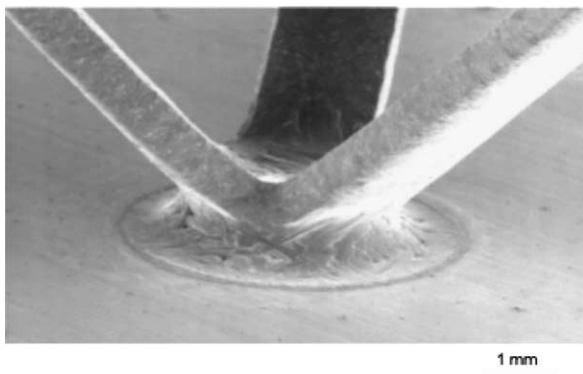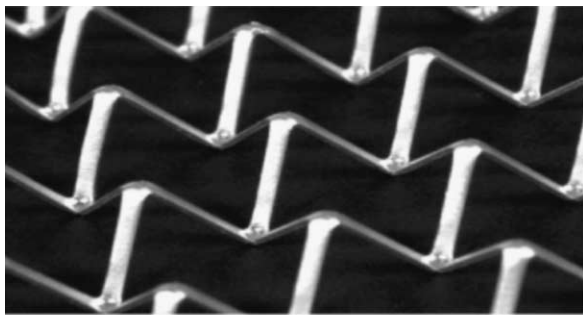

Fig. 6. Example of a tetrahedral truss core layer (top) and a representative transient liquid phase bonded node (bottom).The truss core was made from 304 stainless steel. The core relative density was 1.8%. A Ni 25Cr 10P alloy was used for bonding.

Cellular structures can be made by stacking the fabric and TLP bonding the nodes [26]. The relative density depends on the wire and cell diameters:

$$\bar{\rho}_c \approx \pi R / \alpha L \tag{1}$$

where $2R$ is the wire diameter, L is the cell diameter and α is a stacking parameter ($\alpha2$) [27]. Periodicity is achieved when there is little dispersion in cell size (Fig. 7 left). Pre-crimping provides a convenient means for precise control of the cell size, especially at low relative density and for making a preform for the pyramidal structure (Fig. 8). Corrugation increases the separation of the layers and reduces the relative density. The resulting structure has a degree of anisotropy controlled by corrugation of the nodes prior to bonding (Fig. 7 right). Sandwich panels can be fabricated from these cores, with the wires oriented at any angle to the face sheet normal,such as the 0/90 and ±45 configurations depicted in Figs. 7 and 9 respectively.
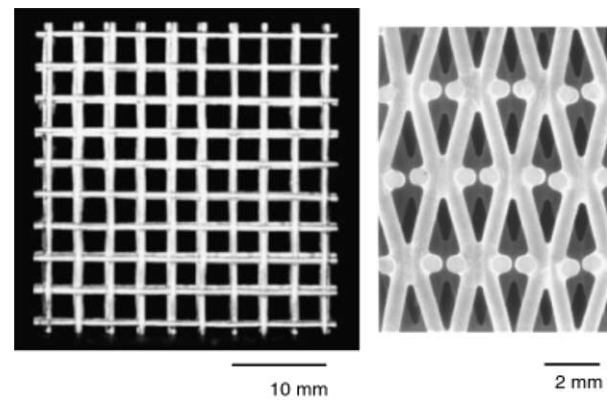

Fig. 7. An inconel textile core viewed from the front (left) and side (right). The core relative density was 18%.
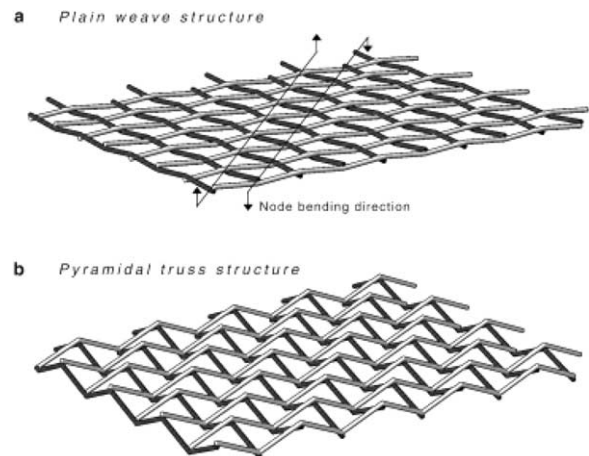

Fig. 8. A plain weave fabric can be sheared and node bonded to create a sheet suitable for bending to create a pyramidal core.

2.3.2. Non-woven approaches

Similar topologies can be fabricated by a wire lay up process followed by transient liquid phase bonding or resistance welding. Using a slotted tool to control wire spacing and orientation it is a simple matter to lay down collinear wires and to alternate the direction between successive layers. This procedure results in square or diamond core topologies that can be machined and bonded to face sheets. The approach has a number of attractions. Relative to the textile approach, it is more straightforward to maintain the cell alignment throughout the structure and less material is wasted (by cropping). Moreover, pre-crimping is not required to achieve very low-density cores. These benefits all reduce the ultimate cost. It is also possible to use hollow tubes instead of wires. Out of plane node bending allows these lay ups to be converted to pyramidal truss topologies. Other truss topologies with hollow ligaments also appear feasible. Preliminary work suggests hollow truss structures might be the strongest identified to date [28].

3. Topology Design for High Strength

Cores suitable for lightweight/multifunctional application use the principle that, when incorporated into a panel subject to shear, the core members stretch/com-

Fig. 9. An example of a diamond orientation, 304 stainless steel textile sandwich panel. The core relative density was 12.6%.
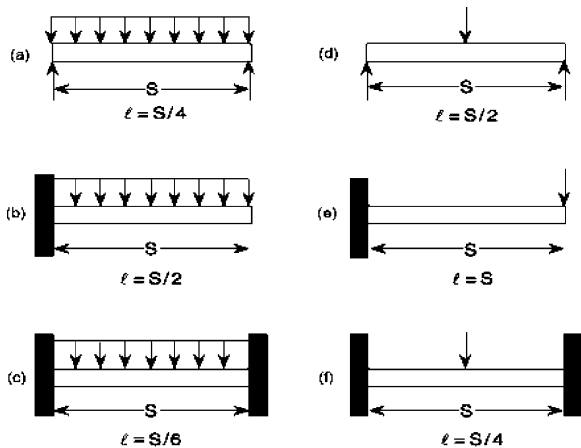

Fig. 10. Relationship between l and loading span S for common test configurations, with (a–c) uniformly distributed pressure, and (e–f) concentrated loads [27].

press without bending [18,21,29]. The basic attributes can be ascertained by analyzing the minimum weight of panels subject to either bending or axial compression that support specified loads without failure [29,27]. When the core and face sheets are made of the same material, the results can be represented in non-dimensional coordinates, which allow comparison between concepts.

In a structure subject to bending, supported over a span, S, the load index combines the sustainable bending moment, M, and transverse shear, V (both per unit width) in the non-dimensional form [29]:

$$\Pi = \frac{V}{\sqrt{EM}} \tag{2}$$

where E is the Young's modulus of the fully dense solid. The ratio $l = M/V$ defines a characteristic length scale related to the loading span, S (see Fig. 10). The corresponding weight per unit width, W, can be expressed in the non-dimensional form:

$$\Psi = \frac{W}{\rho l^2} \tag{3}$$

where ρ is the density of the constituent material. The same coordinate system applies for panels in axial compression.

To ascertain the minimum weight, all potential failure modes must be characterized [1,29]. These modes include face yielding and wrinkling, as well as core member yielding and buckling. Minimum weight designs (Fig. 11) reveal that truss and textile cores with bend resistant topologies have structural performance at least as good as the (benchmark) honeycomb core system [27,29]. Additional benefits of truss/textile cores over
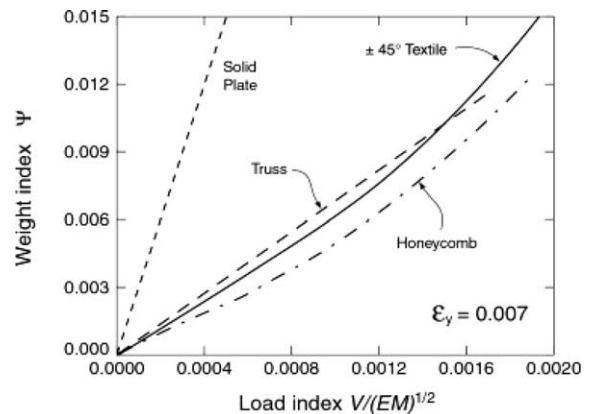

Fig. 11. Minimum weights of panels in bending as a function of load index. A comparison is made between solid plates and sandwich plates with tetrahedral truss cores, hexagonal honeycomb cores and ±45 textile cores, subject to the constraint that the core thickness should not exceed a maximum allowable, $H_c/l \leqslant 0.1$. The operative failure mechanisms are indicated [27].

honeycombs reside in potentially lower manufacturing cost, especially in curved configurations, and in multi-functionality [17].

4. Structural characterization

To construct Fig. 11, models are needed for the dependence of the mechanical properties of the core and the faces upon the topology and relative density. Analytic models augmented by selected finite element simulations are appropriate for this purpose. The approach is illustrated by results for the tetrahedral core with relative density expressed by [18,21]:

$$\bar{\rho}_c = \frac{6\pi R_c^2}{\sqrt{3} L_c H_c} \tag{4}$$

where L_c is the truss length, R_c its radius and H_c the core thickness.

The basic models combine mechanisms governing core failure by yielding/buckling with face failure by yielding/wrinkling. They regard the core and faces as elastic/perfectly plastic [27,29]. The extra load capacity enabled by strain hardening is incorporated at a later stage [22,31]. Near-optimal designs are rarely limited by the compressive strength of the core [21,27]. The ensuing assessment emphasizes the performance-limiting shear response.

4.1. Core failure

The relationship between the axial stress in the core members, σ_z, and the shear force per unit length V:

$$\sigma_z = \frac{\sqrt{3}}{\pi} V \frac{L_c}{R_c^2} \sqrt{\left(\frac{L_c}{H_c}\right)^2 - 1} \tag{5}$$

provides the basis for assessing V at core failure. Equating σ_z to the yield strength of the members, σ_Y, gives V upon *core yielding*:

$$V_Y = \frac{\pi}{\sqrt{3}} \sigma_Y \frac{R_c^2}{(L_c/H_c)^2 - 1} \tag{6}$$

Equating σ_z to the elastic buckling stress [29] gives V for *buckling*:

$$V_B = \frac{\pi^3}{4\sqrt{3}} kE \frac{R_c^4}{H_c L_c^2 \sqrt{(L_c/H_c)^2 - 1}} \tag{7}$$

In (7), k is governed by the rotational stiffness of the nodes. In near-optimal designs, the nodes behave as if they were pin-jointed, $k \approx 1$ [22].

4.2. Failure in the faces

The face failure modes are dictated by the bending moment, M. For a face sheet of thickness, t_f, face *yielding* occurs when [1],

$$M_Y = t_f H_c \sigma_Y \tag{8}$$

Face *wrinkling* occurs when [29]:

$$M_w = 1.12E \frac{t_f^3}{H_c[(L_c/H_c)^2 - 1]} \tag{9}$$

4.3. Scaling

It is convenient to re-define the length parameters in the non-dimensional forms: $x_1 = t_f/l$, x_2, R_c/l, $\eta = L_c/R_c$. In the truss orientation that affords the lowest weight, $L_c/H_c\sqrt{3/2}$ [29]. Then, the weight of the plate is:

$$\Psi = 2x_1 + 2\sqrt{3}\pi \frac{x_2}{\eta} \tag{10}$$

An optimization determines the minimum weight that resists failure, subject to a prescribed combination of M and V.

4.4. The constraints

The constraints are dictated by the four failure modes (6 through 9), re-normalized as:

$$\sqrt{\frac{3}{2}}\Pi^2\left(\frac{1}{\varepsilon_Y \eta x_1 x_2}\right) \leqslant 1 \qquad \text{Face yielding} \tag{11a}$$

$$\frac{\sqrt{3}}{1.12}\Pi^2\left(\frac{\eta x_2}{x_1^3}\right) \leqslant 1 \qquad \text{Face wrinkling} \tag{11b}$$

$$\sqrt{\frac{3}{2}}\Pi^2\left(\frac{\eta}{x_2 \varepsilon_Y}\right) \leqslant 1 \qquad \text{Core yielding} \tag{11c}$$

$$\sqrt{\frac{3}{2}}\frac{4}{\pi^3}\Pi^2\left(\frac{\eta^3}{x_2}\right) \leqslant 1 \qquad \text{Core buckling} \tag{11d}$$

4.5. Minimum weight

Equating core yielding and buckling (11c and d) indicates that for materials with a yield strain of 0.07, buckling occurs in preference to yielding whenever $\eta \geqslant 30$ which is the range applicable to lowest weight designs. The minimum occurs at the confluence of the remaining three mechanisms [1,29]. Sequentially equating (11a,b

and c) and invoking (11a), specifies three equations with three unknowns (x_1, x_2, η). The ensuing face and core thickness and truss aspect ratio are plotted on Fig. 12. Inserting these into (10) then gives the minimum weight Φ_{min} as a function of Π and E_Y. The result is plotted on Fig. 11, subject to the additional constraint that the core thickness should not exceed a maximum allowable, $H_c/l \leqslant 0.1$ Over the practical range of load index, the minimum weight design corresponds to a relative density, $\bar{\rho}_c \approx 0.02$ [27].

5. Comparisons between cores

The compressive and shear characteristics of various cores are compared using combinations of measurements, analytic results and numerical simulations. The picture is incomplete. It is also asymmetric, in the sense that different levels of understanding exist for compression and shear. The following synopsis represents a best attempt at compiling information available at this juncture. The deficiencies identified in this assessment provide a focus for the new measurements, analysis and calculations needed to establish a more complete understanding.
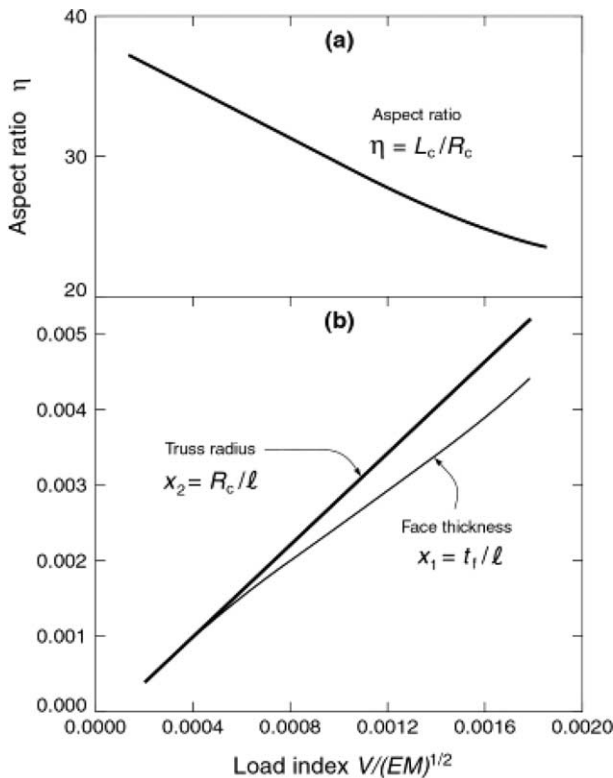

Fig. 12. Constituent dimensions relevant to an optimized tetrahedral truss core panel: (a) aspect ratio of the truss members and (b) the truss radius and the face thickness. Note that the aspect ratio varies minimally with the required load capacity, whereas the radius and thickness increase substantially. The final choice of dimensions is dictated by the largest load that needs to be supported.

5.1. Compressive responses

The elastic properties are relatively well characterized. The honeycomb (hexagonal or square section) realizes the optimal value of through-thickness Young's modulus, $\bar{E}$:

$$\bar{E} = \bar{\rho}_c E \qquad (12)$$

Pyramidal, tetrahedral and triangular cores have $\bar{E}$ diminished by a factor φ, which scales with the angle of inclination ω as:

$$\varphi = \sin^4 \omega \qquad (13)$$

That is, for struts inclined at 45°, $\bar{E}$ is reduced by a factor 4.

The rules governing the load capacity are more complex. The relevant strengths include initial yield, σ_{cY}, the maximum load capacity, σ_{max} (based on plastic and elastic buckling) and the load retention beyond buckling, σ_o (Fig. 13). The maximum, σ_{max} is imperfection sensitive, especially for prismatic topologies. From a design and robustness perspective, the appropriateness of relying on the peak, σ_{max}, rather than the plateau, σ_o, needs further assessment.

The load capacity connects with the constituent material properties through the Ramberg–Osgood stress/strain representation:

$$\varepsilon = \sigma/E + \varepsilon_Y(\sigma/\sigma_Y)^N \qquad (14)$$

where N is the strain hardening exponent and (σ_Y, ε_Y), are the yield strength and yield strain, respectively. Stress/strain curves for the materials used to evaluate the concepts are summarized on Fig. 14. These include cast Cu/Be, 316 stainless steel and an aluminum alloy.
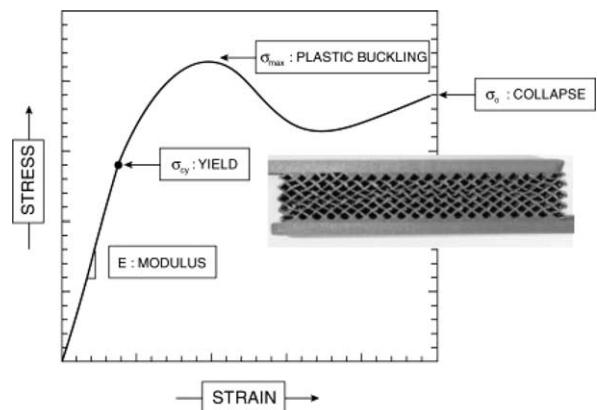

Fig. 13. A schematic of a compressive stress/strain curve indicating the three stress levels of interest. The load drop beyond the peak is associated with plastic buckling. A typical deformed shape is shown on the inset.

Analytic results for loads limited by yielding and elastic buckling establish some of the basics. These are exemplified by results for honeycomb, metal textiles and truss cores, ascertained in the absence of strain hardening (Fig. 15). The transition to elastic buckling (with associated loss in load capacity)occurs for honeycombs at $\bar{\rho}_c \approx 5$. The corresponding transition occurs for truss cores when $\bar{\rho}_c \approx 1$. *The implication is that truss configurations are preferred at low density.*

When the cores fail by yielding,absent imperfections, the strength satisfies (Fig. 15):

$$\bar{\sigma}_{cY} = \varsigma \bar{\rho}_c \sigma_Y \qquad (15)$$

The strongest tetrahedral and pyramidal cores have, $\varsigma = \sin^2\omega \approx 0.7$ while for woven cores, $\varsigma = 0.5$. The honeycombs appear to have the greatest strength, with $\varsigma = 1$. However, their imperfection sensitivity often causes them to deform at much lower stresses, by the axial propagation of plastic folds [30], whereupon:

$$\sigma_{max} \equiv \sigma_o = 3\bar{\rho}_c^{5/3}\sigma_Y. \qquad (16)$$

This imperfection sensitivity downgrades the performance of honeycombs (Fig. 15). It remains to understand circumstances that dictate the relative applicability of (15) and (16) for honeycombs.

Strain hardening elevates the load capacity of truss and textile cores. *Pyramidal* struts having square cross-section, t, and length, l, exhibit plastic buckling at stress,

$$\sigma_{pb} = \frac{\pi^2}{12} E_t \left(\frac{2t}{l}\right)^2 \qquad (17)$$

where E_t is the tangent modulus at σ_{pb} (E_t can be related to the yield strength through (14)). Recalling that the strut aspect ratio, t/l, and inclination, ω, are related to the relative density by:

$$\frac{t}{l} = \left[\frac{\cos^2\omega \; \sin\omega}{2} \bar{\rho}_c\right]^{1/2}, \qquad (18)$$

the plastic buckling stress becomes:

$$\sigma_{pb} = \frac{\pi^2 \; \cos^2\omega \; \sin\omega}{6} \bar{\rho}_c E_t. \qquad (19)$$

Combining with (14), (17)and (18) renders a load capacity renders a load capacity:

$$\sigma_{max} = \sigma_{pb} \bar{\rho}_c \; \sin^2\omega$$
$$\equiv \chi_t(N)\bar{\rho}_c^2 \sigma_Y. \qquad (20)$$

For a *woven* core,with cell size l and wire radius a, the corresponding plastic buckling stress is:

$$\sigma_{pb} = \frac{\pi^2}{4} E_t \left(\frac{a}{l}\right)^2. \qquad (21)$$

The strut aspect ratio is related to the relative density by:

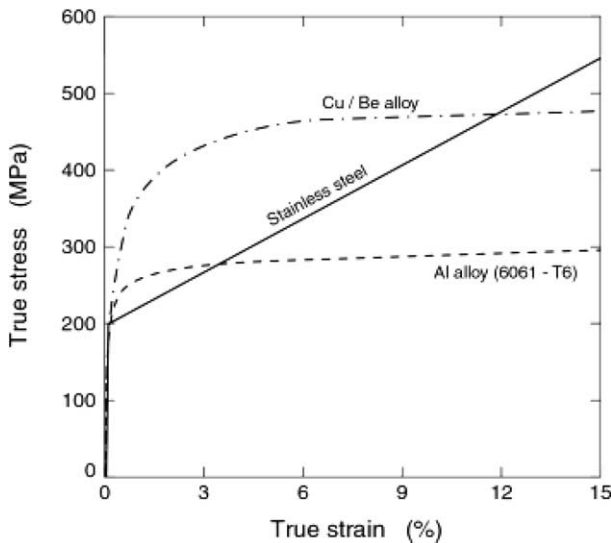$$\frac{a}{l} = \frac{\sin 2\omega}{\pi} \bar{\rho}_c. \qquad (22)$$

Fig. 14. True stress/strain relations for 304 stainless steel (annealed), as cast Cu/1.8%Be and Al 6061-T6.
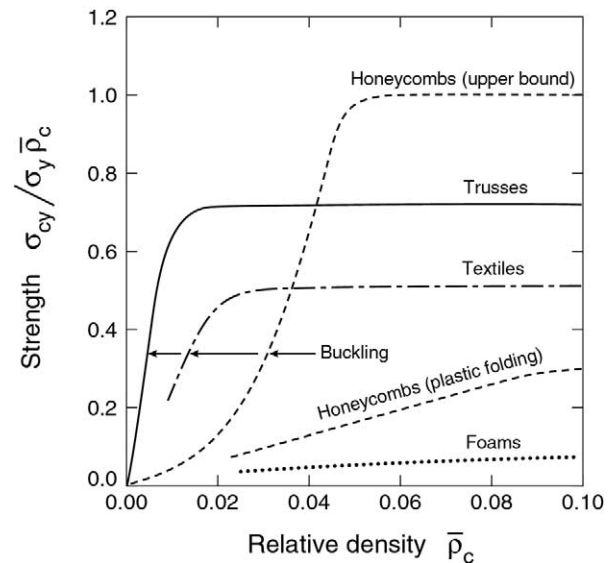

Fig. 15. Comparison of the compressive stresses at yield as a function of relative density for a range of core configurations. The honeycomb results are for crushed (lower curve) and stabilized Hexcel 5052 aluminum honeycomb. The two curves for honeycombs reflect the imperfection sensitivity, as elaborated in the text. The lower curve satisfies the dependence, $\sigma_o = 3\bar{\rho}_c^{3/5}\sigma_Y$. The curve for trusses is an upper bound that occurs when the truss angle is, $\Psi = 57°$: lower values exist for other angles. All of the configurations transition to failure by elastic buckling at low core density. Note that the honeycomb is most susceptible to this transition. Results for aluminum foams are also shown.

whereupon, the bifurcation stress becomes:

$$\sigma_{pb} = \frac{\sin^2 2\omega}{\pi} \bar{\rho}_c^2 E_t \qquad (23)$$

and the load capacity is:

$$\sigma_{max} = \frac{\sin^2 \omega}{2} \bar{\rho}_c \sigma_{pb}$$
$$\equiv \chi_w(N) \bar{\rho}_c^3 \sigma_Y$$

Note that the maximum stress for the woven cores scales as $\bar{\rho}_c^3$, while that for the pyramidal, struts scales with $\bar{\rho}_c^2$. The implication is that, at densities in the practical range, from a peak load capacity perspective, *the trusses should always be superior to textiles.*

Further insight is gained from measurements performed on single layer tetrahedral, textile and honeycomb cores, censored by only including results unaffected by edges which are significant for textile cores (Fig. 16). The measurements for cores with pyramidal, $\chi_t \approx 1.48$ and woven, $\chi_w \approx 0.7$, topologies (Fig. 17a) affirm that the peak strengths *exceed* those associated with yield (15): in some cases substantially (Fig. 17b). It remains to understand the associated fundamentals. The results also affirm that honeycombs tend to fail in accordance with the lower load capacity, defect facilitated plastic folding mechanism (16), rather than plastic yielding (15).

Note that stacking pyramidal cores (Fig. 18) does not change the initial yield load, but the wavelength of the

buckling pattern increases, diminishing the peak load by up to 50% and reducing differences between honeycomb, textiles and trusses (Fig. 17).

5.2. Shear responses

The shear responses of various cores are summarized on Figs. 19–21 [18,31,33]. For comparison purposes, it is convenient to re-express the shear measurements in terms of a core shear strength [18,21]:

$$\tau_Y^c = \xi \sigma_Y \bar{\rho}_c \qquad (25)$$

Fig. 17. Measured values of the compressive response of various core configurations. (a) Stress/strain curves for a pyramidal and textile cores. Note the exceptionally large peak load reached by the pyramidal configuration. (b) Peak stresses measured for several cores compared using the non-dimensional stress, $\sigma_{max}/\sigma_Y\bar{\rho}_c$, plotted as a function of relative density. Note that the results for pyramidal trusses exceed unity. Moreover, for these configurations, as well as for the honeycombs, there is a tendency for the load capacity to increase as the density increases. This trend is believed to be associated with effects of stockiness on the post buckling behavior.
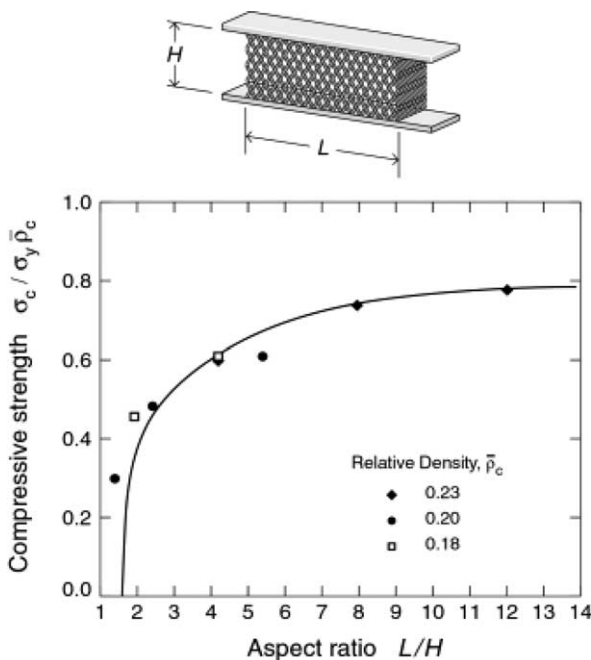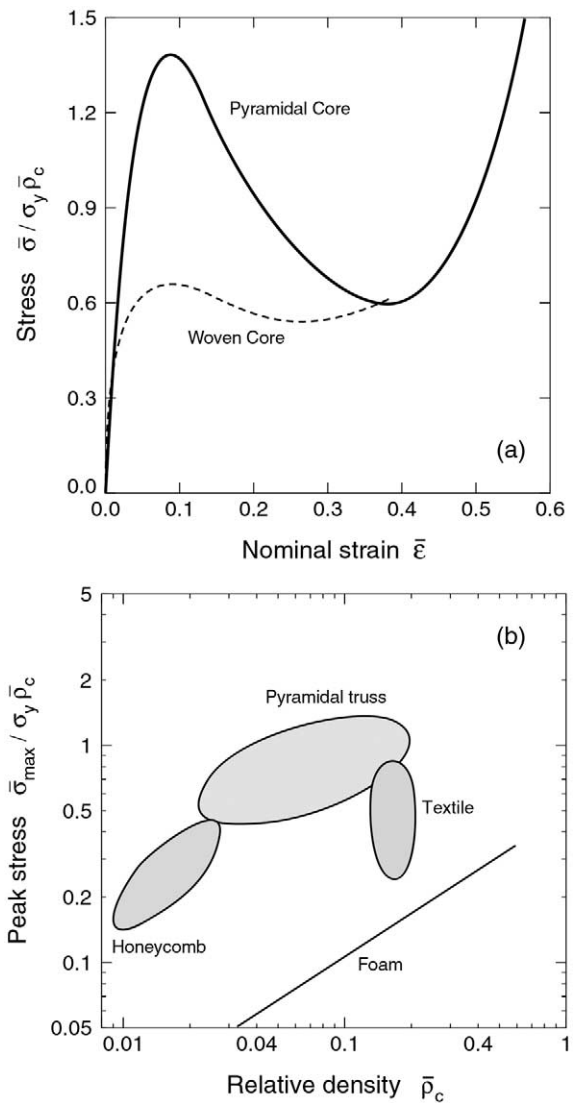

Fig. 16. The effect of aspect ratio on the peak load measured for a textile core. Note that the stress asymptotes to the wide plate strength when the length to thickness ratio satisfies, $L/H > 8$. All other results used in this article refer to tests performed in this range.

Finite element simulations conducted using unit cells with periodic boundary conditions are re shown in the figures [22,32]. The measurements thus far have various limitations. (a) Those performed on investment cast systems have the disadvantage that the plastic deformation prior to rupture at the nodes is quite small [18]. (b) The results on panels with tetrahedral cores made using the constructed metal lattice approach [25,32,33] have the limitation that the member cross sections are rectangular (and thus sub-optimal for plastic buckling). (c) The tests on textile cores have been confined to relative large core densities [26,31,34]. Subject to these limitations, the following generalizations can be made about the responses at small-to-moderate plastic strains ($<10\%$).
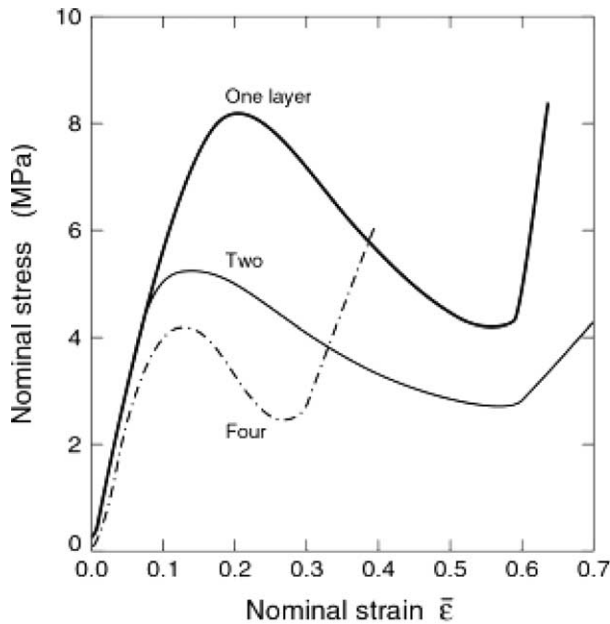

Fig. 18. The effect of multiple layers of the pyramidal core on the stress/strain curve. Note that the layering introduces imperfections that reduce the peak load quite appreciably.
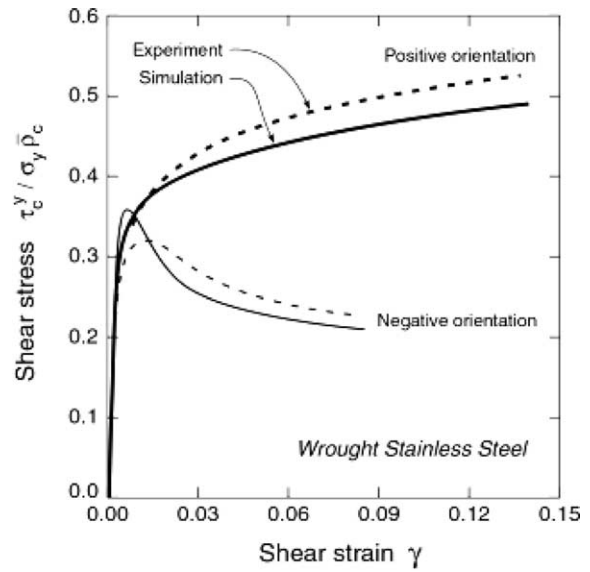

Fig. 20. The shear stress/strain curves for a tetrahedral truss core panel made from stainless steel using the constructed metal approach. Measurements made in the positive and negative orientations are shown as well as simulations performed using the stress/strain curve plotted on Fig. 14.
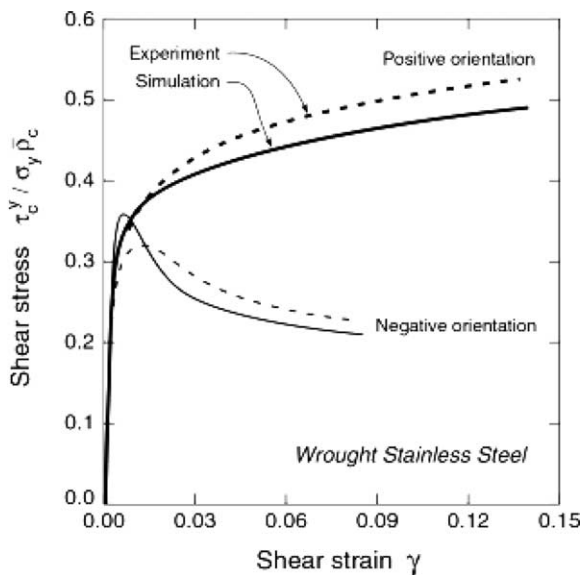

Fig. 19. The shear stress/strain curves for a tetrahedral truss core panel made from Cu/Be alloy by investment casting. Measurements made in the positive and negative orientations are shown as well as simulations performed using the stress/strain curve for the alloy plotted on Fig. 14. The truss members have circular cross section with relative density, $\bar{\rho}_c = 2.25\%$.
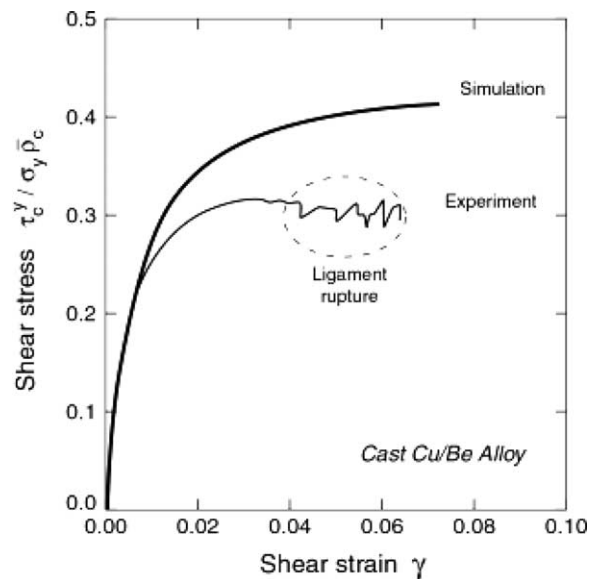

Fig. 21. The shear stress/strain curves for a 3D Kagome truss core panel made from Cu/Be alloy by investment casting. A comparison between measurement and simulation is shown for tests performed in one orientation. Results in all other orientations are essentially the same. The truss members have the circular cross section with relative density, $\bar{\rho}_c = 2.25\%$.

5.2.1. Topology

The ±45 textile cores exhibit initial yield at $\xi \rightarrow 0.78$. However, these cores are anisotropic with appreciably lower strength in the orthogonal orientation. The 3D Kagome core is isotropic with $\xi \rightarrow 0.45$. The tetrahedral and pyramidal truss cores are nearly isotropic with $\xi \rightarrow 0.32$ in the weakest orientation.

5.2.2. Strain hardening

For each topology, ξ at peak load is governed by core members that fail by plastic buckling (Fig. 22). This effect causes the tetrahedral core to be asymmetric (Fig. 20). In the negative orientation (one member in compression), plastic buckling, followed by softening, occurs when $0.32 \leqslant \xi \leqslant 0.38$, with a strong dependence on strain hardening. In the positive orientation (two members in compression), the response is dominated by the stretching of the member in tension such that $0.39 \leqslant \xi \leqslant 0.52$, again dependent on strain hardening.

5.2.3. Simulations

The finite element simulations and measurements in domains controlled by plastic buckling are remarkably consistent (Figs. 18–20). The simulations slightly overestimate the peak load (because of imperfection effects)
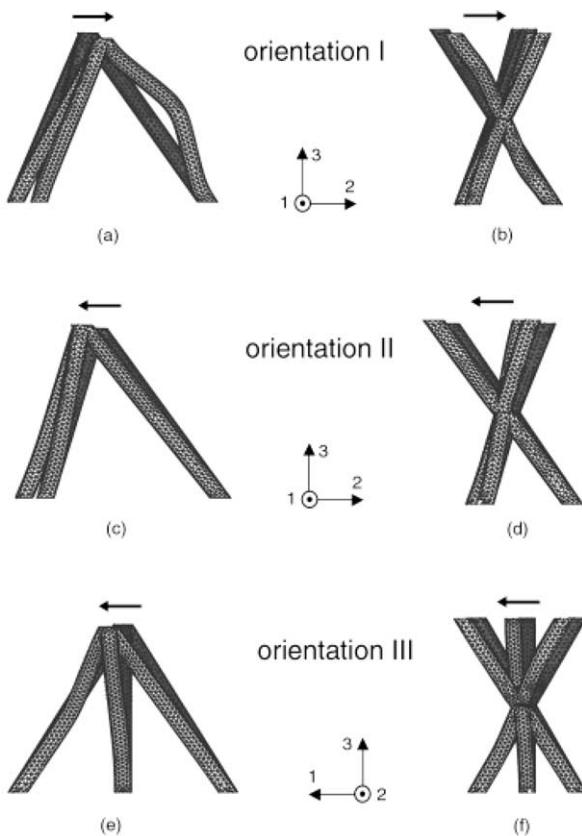

Fig. 22. The displacements of the truss members determined using finite element simulations corresponding to the stress/strain curves measured in the negative orientation.

but otherwise, capture all aspects of the shear stress/strain curve.

5.2.4. Elastic buckling

None of the configurations tested to date have a low enough core density to have failed by elastic buckling.

5.3. Beam tests

Tests performed on beams in 3-point bending have been designed to probe failure by core shear and face yielding. Failures by core buckling and face wrinkling have yet to be explored. The test protocol is guided by analytic estimates of the load capacity of the panels.
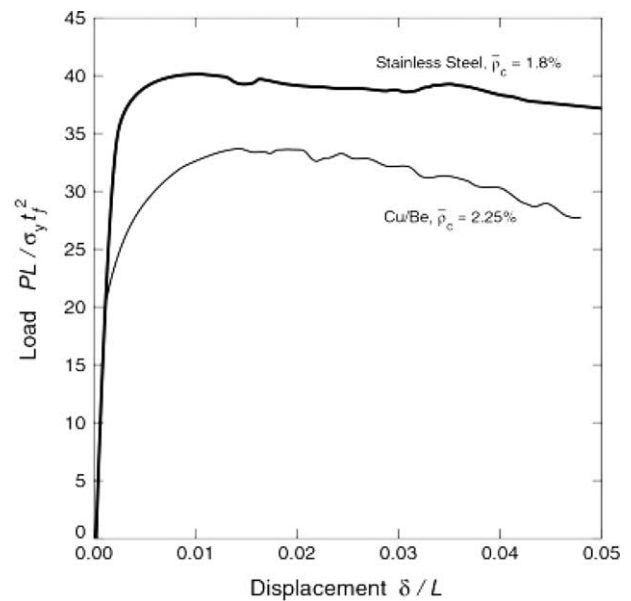

Fig. 23. Load/deflection curves measured in bending for tetrahedral truss core panels made from stainless steel using the constructed metal approach.
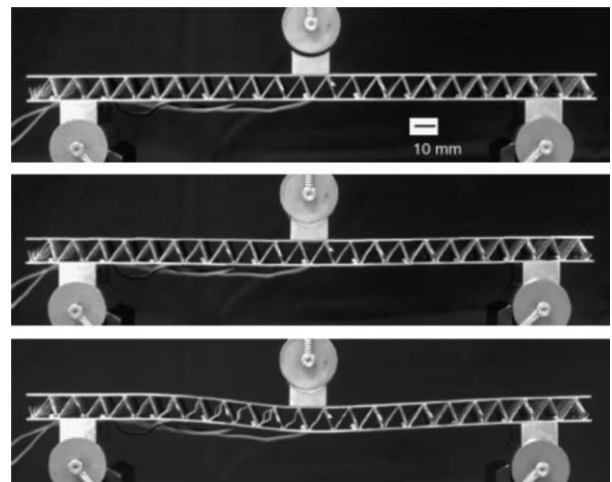

Fig. 24. Images of a constructed-metal, stainless steel, panel at three displacements incurred during the bending test expressed in Fig. 23.

When *core shear* predominates, the response at the outer supports has an important influence. If plastic hinges develop across the section of the sandwich beam at the outer supports, the overhang does not contribute to that portion of the load carried by the core, and the maximum load per unit width becomes [1]:

$$P_{max}^{core} = \frac{4t_f^2\sigma_Y}{S} + 2H_c\tau_Y^c \tag{26a}$$

The first term is the contribution from the plastic hinges formed in the faces and the second due to shear yielding of the core. Absent hinges at the supports, the corresponding result is:

$$P_{max}^{core\cdot} = \frac{2t_f^2\sigma_Y}{S} + 2H_c\tau_Y^c[1 + 2H_{over}/S] \tag{26b}$$

where H_{over} is the overhang of beam beyond each of the outer supports. When the panel fails by *face yielding*:

$$P_{max}^{face} \approx \frac{4t_f(H_c + t_f)\sigma_Y}{S} \tag{26c}$$

The results of bending tests performed under conditions wherein either (26a) or (26b) apply are summarized in Figs. 23 and 24. Several features emerge.

5.3.1. Assymetry
The limit loads are governed by core shear in the negative orientation (Fig. 24). Plastic buckling of those core members in compression is evident on the left side of the test specimen.

5.3.2. Robustness
Despite the softening experienced by the buckled trusses on the left of Fig. 24, the plates retain their load capacity (Fig. 23). This happens because the core struts are sufficiently stocky. Even the cast plate, which exhibits brittle failure of some of the nodes, demonstrates sustained load capacity; it is surmised that the failed truss members shed load to other parts of the structure.

5.3.3. Scaling
The plate made from Cu/Be is stronger than that made from stainless steel, but lower when normalized by the yield strength. The interpretation is as follows. (a) The stainless steel plate has a lower $\bar{\rho}_c$, reducing the load capacity of the core by about 20%. (b) The stainless steel trusses have a rectangular (rather than circular) cross section, resulting in a lower resistance to plastic buckling by a factor ~0.75. The comparison suggests that, for the identical topology, density and yield strength, the panel made by the constructed metal approach exhibits the greater load retention beyond the load maximum.

5.3.4. Load capacity
Estimates of the limit load based on (26) all underestimate the measured values when ξ representative of the weakest orientation is used [18,31,27]. The discrepancies are believed to be due to load redistribution and strain hardening of the faces. A detailed interpretation through simulation awaits appropriate constitutive laws for the cores, now under development [35,36].

6. Concluding comments

It has been demonstrated that robust metallic sandwich panels with periodic, open cell, cores can be fabricated using protocols based both on the sheet forming of trusses and textile assembly. Analysis, testing and optimization have revealed that sandwich panels constructed with these cores sustain loads at weights greatly superior to stochastic foams and competitive with the lightest known (honeycomb core)systems. The benefits of the truss/textile cores over honeycombs reside in their higher specific strength at low relative density, and lower manufacturing cost, as well as in their multifunctionality [37,38,39]. Their open cell structure allows for heat transfer into a coolant fluid, for the storage of electrical energy as a battery (with the core as one of the electrodes),for acoustic absorption, inter alia.

References

[1] Ashby MF, Evans AG, Fleck NA, Gibson LJ, Hutchinson JW, Wadley HNG. Metal foams: a design guide. Boston: Butterworth Heinemann; 2000.
[2] Wadley HNG. Cellular metals manufacturing. Advanced Engineering Materials 2002;4(10).
[3] Banhart J. Progress in Materials Science 2001;46:559–632.
[4] ERG, Inc., Oakland USA, DUOCEL product data sheet, www.ergaerospace.com, 2000.
[5] Grohn M, Voss D, Hintz C, Sahm PR. In: Barnhart J, Ashby MF, Fleck N, editors. Cellular Metals and Metal Foaming Technology. MIT-Verlag; 2001. p. 197–202.
[6] INCO Ltd, Canada, Incofoam Data Product Sheet, www.inco.com, 1998.
[7] Frame C. url: www.porvair.com, 2000.
[8] Jackel M. German Patent DE 3,210,770, 1983.
[9] Nagel AR, Uslu C, Lee KJ, Cochran JK, Sanders TH. Mat Res Soc Symp Proc 1995;372:155–63.
[10] Sypeck DJ, Parrish PA, Wadley HNG. Mat Res Soc Symp Proc 1998;521:205–10.

[11] Chen F, He D. In: Banhart J, Ashby MF, Fleck NA, editors. Metal Foams and Porous Metal Structures. MIT-Verlag Bremen; 2001. p. 163–6.

[12] Sugimura Y, Meyer J, He MY, Bart-Smith H, Grenestedt J, Evans AG. Acta Mater 1997;45(12):5245–59.

[13] Baumgartner F, Kruschek H, Schwalbe HF, Nijhof K. In: Banhart J, Ashby MF, Fleck NA, editors. Metal Foams and Porous Metal Structures. MIT-Verlag Bremen; 2001. p. 283–8.

[14] Barnhart J, Baumeister J. M Weber Mat Sci Eng 1996;A205:221.

[15] Lu TJ, Stone HA, Ashby MF. Acta Mater 1998;46:3619–35.

[16] Pestryakov AN, Lunin VV, Devochkin AN, Petrov LA, Bogdanchikova NE, Petranovskii VP. Applied Catalysis A: General 2002;227:125–30.

[17] Evans AG. MRS Bull 2001;26(10).

[18] Chiras S, Mumm DR, Evans AG, Wicks N, Hutchinson JW, Dharmasena KP, Wadley HNG, Fichter S. Int J Solids Struct 2002;39:4093–415.

[19] Bitzer T. Honeycomb Technology. Chapman & Hall; 1997.

[20] Wadley HNG. Advanced Engineering Materials 2002;4(10):726–33.

[21] Dehpande VS, Fleck NA. Int J Solids Struct 2001;38:6275.

[22] Wang J, Evans AG, Dharmasena KP, Wadley HNG. Int J Solids Struct (in press).

[23] Jonathon Aerospace Materials website (www.jamcorp.com).

[24] Krause DL, Whittenberger JD, Kantzos PT, Hebsur MG. Mechanical testing of IN718 Lattice Block Structures, NASA TM-2002-211325.

[25] Sypeck DJ, Wadley HNG. In: Banhart J, Ashby M, Fleck N, editors. Cellular Metals and Metal Foaming Technology. Bremen: Verlag MIT; 2001. p. 381–6.

[26] Sypeck DJ, Wadley HNG. J Mater Res 2001;16(3):890–7.

[27] Zok FW, Rathbun HJ, Wei Z, Evans AG. Int J Solids Struct. Submitted, 2003.

[28] Queheillalt D. Private Communication, 2003.

[29] Wicks N, Hutchinson JW. Int J Solids Struct 2001;38:5183–6165.

[30] Wierzbicki T. Int J Impact Engineering 1983;1(2):157–74.

[31] Mumm DR, Chiras SJ, Evans AG, Hutchinson JW, Sypeck DJ, Wadley HNG. J App Mech, Submitted, 2003.

[32] Rathbun H, Zok F, Evans AG, Sypeck D, Wadley HGN. J App Mech, in press.

[33] Zupan M, Chen C, Fleck NA. The compressive response of a sandwich plate with a core of tetrahedral lattice material, manuscript in preparation, 2003.

[34] Zupan M, Deshpande VS, Fleck NA. The compressive response of a stacked assembly of woven steel, manuscript in preparation.

[35] Chen C, Deshpande VS, Fleck NA. A transversely isotropic constitutive model for a foam. Manuscript in preparation, 2003.

[36] Vaughn and Hutchinson, in preparation.

[37] Evans AG, Hutchinson JW, Ashby MF. Multifunctionality of cellular metal systems. Progress in Materials Science 1999;43:171–221.

[38] Evans AG, Hutchinson JW, Fleck NA, Ashby MF, Wadley HNG. Progress in Mat Science 2001;46:309–27.

[39] Tian J, Kim T, Lu TJ, Hodson HP, Sypeck DJ, Wadley HNG, submitted.